Prepared for submission to JCAP

Cosmogenic radionuclide production in NaI(Tl) crystals

J. Amaré, S. Cebrián, C. Cuesta,[1] E. García, C. Ginestra, M. Martínez, M.A. Oliván, Y. Ortigoza, A. Ortiz de Solórzano, C. Pobes,[2] J. Puimedón, M.L. Sarsa, J.A. Villar and P. Villar

Laboratorio de Física Nuclear y Astropartículas, Universidad de Zaragoza
Calle Pedro Cerbuna 12, 50009 Zaragoza, Spain
Laboratorio Subterráneo de Canfranc
Paseo de los Ayerbe s/n, 22880 Canfranc Estación, Huesca, Spain
E-mail: amare@unizar.es, scebrian@unizar.es, ccuesta@unizar.es, edgarcia@unizar.es, cginestra@unizar.es, mariam@unizar.es, maolivan@unizar.es, ortigoza@unizar.es, alfortiz@unizar.es, cpobes@unizar.es, puimedon@unizar.es, mlsarsa@unizar.es, villar@unizar.es, pvillar@unizar.es

Abstract. The production of long-lived radioactive isotopes in materials due to the exposure to cosmic rays on Earth surface can be an hazard for experiments demanding ultra-low background conditions, typically performed deep underground. Production rates of cosmogenic isotopes in all the materials present in the experimental set-up, as well as the corresponding cosmic rays exposure history, must be both well known in order to assess the relevance of this effect in the achievable sensitivity of a given experiment. Although NaI(Tl) scintillators are being used in experiments aiming at the direct detection of dark matter since the first nineties of the last century, very few data about cosmogenic isotopes production rates have been published up to date. In this work we present data from two 12.5 kg NaI(Tl) detectors, developed in the frame of the ANAIS project, which were installed inside a convenient shielding at the Canfranc Underground Laboratory just after finishing surface exposure to cosmic rays. The very fast start of data taking allowed to identify and quantify isotopes with half-lives of the order of tens of days. Initial activities underground have been measured and then production rates at sea level have been estimated following the history of detectors; values of about a few tens of nuclei per kg and day for Te isotopes and ^{22}Na and of a few hundreds for I isotopes have been found. These are the first direct estimates of production rates of cosmogenic nuclides in NaI crystals. A comparison of the so deduced rates with calculations using typical cosmic neutron flux at sea level and a carefully selected description of excitation functions will be also presented together with an estimate of the corresponding contribution to the background at low and high energies, which can be relevant for experiments aiming at rare events searches.

Keywords: Cosmic-rays, radionuclide production, NaI detectors, dark matter

arXiv:1411.0106v2 [physics.ins-det] 16 Jan 2015

[1]Present address: Center for Experimental Nuclear Physics and Astrophysics, and Department of Physics, University of Washington, Seattle, WA, USA
[2]Present address: Instituto de Ciencia de Materiales de Aragón, Universidad de Zaragoza - CSIC

Contents

1 Introduction **1**

2 Experimental set-up and measurements **3**

3 Data analysis and estimate of production rates at sea level **6**
3.1 Initial activities underground 9
3.1.1 I and metastable Te isotopes 9
3.1.2 ^{121}Te 9
3.1.3 ^{22}Na 11
3.2 Estimate of production rates at sea level 12

4 Calculation of production rates at sea level **15**
4.1 Excitation functions 16
4.2 Cosmic rays spectrum 18
4.3 Production rates 18

5 Contribution to detector background levels **19**

6 Conclusions **20**

A Excitation functions **26**

1 Introduction

Production of radioactive isotopes by exposure to cosmic rays is a well known issue [1]. Several cosmogenic isotopes are important because of their broad applications in extraterrestrial and terrestrial studies dealing with astrophysics, geophysics, paleontology and archaeology. For experiments searching for rare phenomena like the nuclear Double Beta Decay or the interaction of Weakly Interacting Massive Particles (the so-called WIMPs, which could be filling the galactic dark matter halo) requiring detectors working in ultra-low background conditions, long-lived radioactive nuclei induced in materials of the set-up can be a sensitivity limiting hazard. Operating in deep underground locations, using active and passive shields and selecting carefully radiopure materials for the building of the detectors and shields are common practices in this kind of experiments to reduce very efficiently the background entangling the searched signal [2, 3]. Cosmogenic radionuclides produced during fabrication, transport and storage of components may be even more important than residual contamination from primordial nuclides and become very problematic, depending on the target. For instance, the poor knowledge of cosmic ray activation in detector materials is highlighted in [4] as one of the three main uncertain nuclear physics aspects of relevance in the direct detection approach pursued to solve the dark matter problem.

One of the most relevant processes in cosmogenic activation is the spallation of nuclei by high energy nucleons, but other reactions like fragmentation, induced fission or capture can be very important for some nuclei. Cosmogenic activation is strongly dependent on the nucleon flux, neutron to proton ratio, and energies available. At sea level, for instance, the flux of neutrons and protons is virtually the same at a few GeV, but the proton to neutron ratio

decreases significantly at lower energies because of the charged particles absorption in the atmosphere. For example, at 100 MeV this ratio is about 3% [1]. Summarizing, at sea level, nuclide production is mainly dominated by neutrons at low energies, whereas if materials are flown at high altitude cosmic flux is much greater, energies at play are larger and activation by protons can not be neglected.

In principle, cosmogenic activation can be kept under control by minimizing exposure at surface and storing materials underground, avoiding flights and even using shields against the hadronic component of cosmic rays during surface operation. But since these requirements usually complicate the preparation of experiments (for example, while crystal growth and detectors mounting steps) it would be desirable to have reliable tools to quantify the real danger of exposing the different materials to cosmic rays. Direct measurements, by screening of exposed materials in very low background conditions as those achieved in underground laboratories, and calculations of production rates and yields, following different approaches, have been made for several materials in the context of dark matter, double beta decay and neutrino experiments (see for instance [5] and references therein). Many different studies are available for germanium [6]-[12] and interesting results have been derived also for copper [12, 13], stainless steel [14], tellurium [15, 16] or neodymium [17, 18]. However, systematic studies for other targets are missed.

Sodium iodide crystals (Tl doped) have been widely used as radiation detectors profiting from the very high light output [19, 20]. In particular, NaI(Tl) detectors have been applied in the direct search for dark matter for a long time [21]-[26]. Among the several experimental approaches using NaI(Tl) detectors, DAMA/LIBRA is the most relevant, having reported the observation of a modulation compatible with that expected for galactic halo WIMPs with a large statistical significance [27]. Results obtained with other target materials and detection techniques have been ruling out for years the most plausible compatibility scenarios. The ANAIS (Annual modulation with NaI Scintillators) project [28] is intended to search for dark matter annual modulation with ultrapure NaI(Tl) scintillators at the Canfranc Underground Laboratory (LSC) in Spain; the aim is to provide a model-independent confirmation of the annual modulation positive signal reported by DAMA/LIBRA using the same target and technique. Several prototypes have been developed and operated in Canfranc [29]-[32]. Projects like DM-Ice [33], KIMS [34] and SABRE [35] also envisage the use of large masses of NaI(Tl) for dark matter searches. However, complete understanding of the DAMA/LIBRA background at low energy has not yet been achieved and some open questions remain [36, 37]; therefore, careful analysis of the different background components is highly recommended. In the case of ANAIS, a successful background model was built for previous prototypes (ANAIS-0) [29], but ANAIS-25 background is not completely explained by a similar background model [38]. Hence, other possible background contributions have to be included into the model, and in particular, we address in this work the cosmogenic contribution.

For NaI, production of ^{129}I, ^{125}I and ^{22}Na was analyzed in [39] in the context of the DAMA/LIBRA experiment and the presence of cosmogenic isotopes has been also reported by ANAIS [38, 40], DM-Ice [33] and KIMS [34] collaborations. In this work, cosmogenic yields induced on the Earth surface in two large NaI(Tl) crystals produced by Alpha Spectra[1] for the ANAIS experiment have been quantified; results presented here come from the so-called ANAIS-25 set-up [38]. The ultra-low background conditions of ANAIS and a prompt start of data taking after moving the detectors underground were essential to carry out the analysis

[1] Alpha Spectra Inc., Grand Junction, Colorado, US. http://www.alphaspectra.com/.



Figure 1. Picture of one of the ANAIS-25 detectors (D0), after the coupling of PMTs and placement of the copper casing at the LSC clean room.

of the cosmogenic activation. The structure of the paper is the following. Section 2 describes the experimental set-up and the measurements taken, while the data analysis performed and the production rates at sea level derived for the cosmogenic isotopes identified in the measurements are presented in section 3. A calculation of the corresponding production rates has been attempted using carefully selected excitation functions and the history of the raw material the detectors consist of; such calculations are summarized in section 4, together with the comparison with the experimental rates and corresponding discussion. The impact of cosmogenic products on the background levels at the energy regions relevant for rare event searches is evaluated in section 5. Finally, conclusions are presented in section 6.

2 Experimental set-up and measurements

Two NaI(Tl) detectors built in collaboration with Alpha Spectra form the ANAIS-25 set-up [38]. Each detector consists of a cylindrical 12.5 kg NaI(Tl) crystal, with 4.75" diameter and 11.75" length. They were grown with selected ultrapure NaI powder and encapsulated in OFHC copper with two synthetic quartz windows allowing the coupling to photomultiplier tubes (PMTs) in a second step. Two Hamamatsu R12669SEL2 PMTs were used for one crystal and Hamamatsu R11065SEL PMTs for the other; we will refer to both detectors as D0 and D1, respectively, in the following. Only white Teflon was used as light diffuser, wrapping the crystal, inside the copper encapsulation. A Mylar window allows to calibrate at low energy both detectors. ANAIS-25 detectors are being operated at hall B of LSC under 2450 m.w.e. (meter water equivalent), inside a shielding consisting of 10 cm archaeological lead plus 20 cm low activity lead, all enclosed in a PVC box tightly closed and continuously flushed with boil-off nitrogen. Figure 1 shows a picture of detector D0 and a drawing of the ANAIS-25 set-up is depicted in figure 2.

Each PMT charge output signal is separately processed [38]; each one is divided into a trigger signal, a signal going to the digitizer, and several ones differently amplified/attenuated, and fed into QDC (charge-to-digital converter) module channels to be integrated in a 1 μs window. Low energy (LE) and high energy (HE) ranges, below and above $\sim$200 keV respectively, have been considered in the data analysis presented here. The building of the spectra was done by software (off-line) by adding the signals from both PMTs. Data triggering is done in logical OR mode between the two detectors and in logical AND between the two PMT signals from each detector, at photoelectron level. The outstanding light collection efficiency obtained in ANAIS-25 modules, with measured values of 16.13$\pm$0.66 and 12.58$\pm$0.13 phe/keV for D0 and D1 detectors respectively [38] guarantees a very low energy threshold.

The main goal of ANAIS-25 set-up was to assess the total background of the detectors and, in particular, to determine precisely the ^{40}K content of the crystals, since it was found to be the dominant background in previous ANAIS prototypes [29]. The technique used to

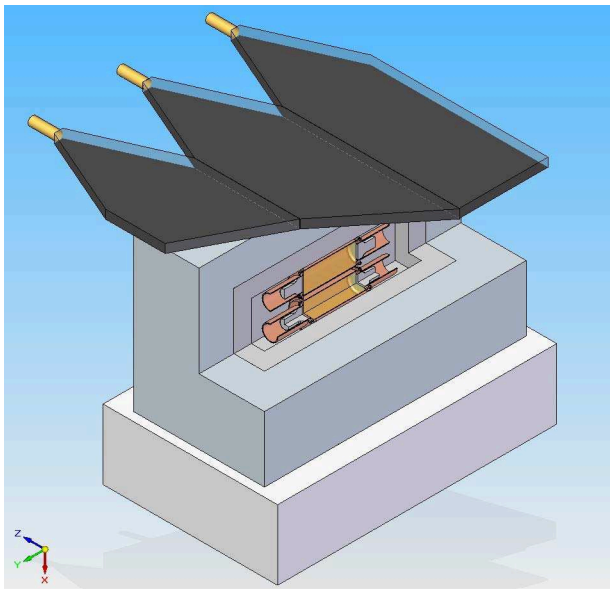


Figure 2. Schematic drawing of the ANAIS-25 experimental layout at LSC, consisting of 10 cm archaeological lead plus 20 cm low activity lead, enclosed in a PVC box continuously flushed with boil-off nitrogen and active vetoes anti-muons.

estimate the bulk ^{40}K activity in the crystals is the measurement in coincidence: one detector measures the total energy (3.2 keV) released by the X-ray/Auger electrons emissions of argon following the K-shell electron capture (EC) of ^{40}K, while the other one measures the fully absorbed energy (1460.8 keV) of the high energy gamma escaping from the former. Averaging the results for the two crystals, an activity of 1.25±0.11 mBq/kg (41.7±3.7 ppb of natural potassium) was derived [30]; this value is one order of magnitude better than that found in other crystals, but still a factor of 2 higher than the required purity. Background assessment is in progress, as far as cosmogenic contribution to the background is still decaying. The excellent light collection efficiency measured in ANAIS-25 modules results in a very good energy resolution which has helped in the identification of cosmogenically produced isotopes.

ANAIS-25 crystals were built in Alpha Spectra facilities in Colorado and then shipped by boat from the US to Spain, avoiding air travel. They arrived at LSC in the evening of 27^{th} November 2012 and were immediately stored underground; data taking started only three days later, after coupling PMTs in the LSC clean room, placing the detectors inside the shielding and preliminary testing of electrical connections and general performance. This prompt commissioning of ANAIS-25 allowed to observe short-lived isotopes and to properly quantify induced activation in those long-lived. Data analyzed for this study correspond to three data sets. Data sets I and II span altogether for 210 days, from the beginning of the data taking to the end of June 2013; we will refer to set I for data obtained until February 2013 and to set II for those taken from March to June 2013. They were acquired in slightly different gain conditions, which implied that some signals present in the LE or HE spectra in one set were not available in the other. Set III includes 88 days of data from March to June 2014, once the contribution of most of the cosmogenic nuclei is significantly reduced, allowing to identify longer-living products.

Figure 3 compares the spectra from D0, both in the low and high energy regions, evaluated in the beginning of data set I and about fifteen months afterwards, during data set III,

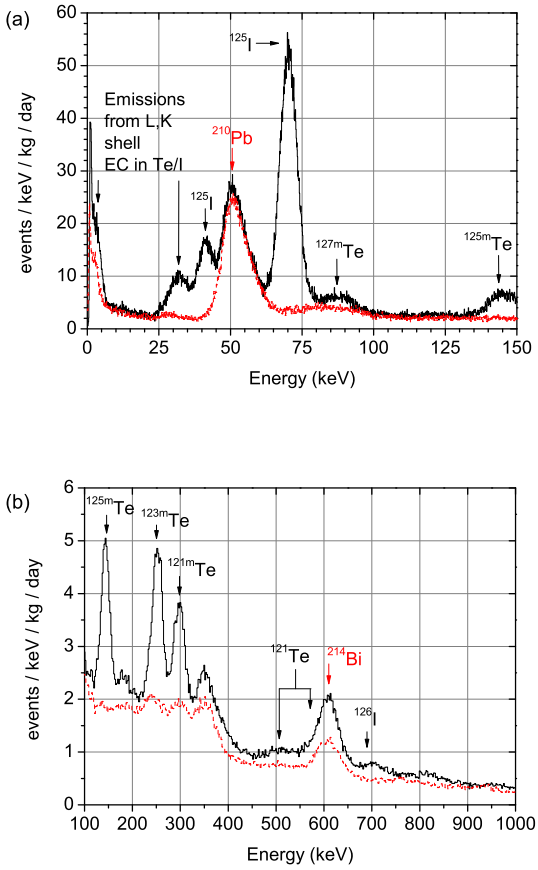


Figure 3. Comparison of the ANAIS-25 spectra evaluated in the beginning of data set I (black solid line) and about fifteen months afterwards, during data set III (red dashed line), over 13.0 and 18.5 days, respectively. The low (a) and high (b) energy regions are shown. Only data from D0 are shown, being those for D1 very similar. Several cosmogenic emissions have been identified and are labeled (see text and table 1). Main background lines are labeled too (in red).

over 13.0 and 18.5 days, respectively. Several lines can be clearly attributed to cosmogenic activation, as figure 3 shows. Iodine and tellurium isotopes identified are presented in table 1; recommended values for half-lives by Decay Data Evaluation Projet (DDEP) [41][2] have been considered for all the analyzed nuclides. Although not directly seen in figure 3, cosmogenically produced ^{22}Na, having a longer mean life than I and Te products, has been identified and quantified using coincidence spectra along data set III.

There are other isotopes, also cosmogenically produced, that have not been identified in this analysis, although they are probably present in ANAIS-25 crystals. It is worth to mention the cases of ^{129}I and ^{123}Te.

^{129}I can be produced by uranium spontaneous fission and by cosmic rays. Its concentration is strongly affected by the ore material exposure either to cosmic rays or to high uranium content environment. It presents 100% β^- decay to the excited level of 39.6 keV of

[2] http://www.nucleide.org/DDEP_WG/Periodes2010.pdf

Isotope	Half-life	Decay mechanism	Main γ emissions / Metastable level energy (keV)	$I\epsilon$
^{126}I	(12.93±0.05) d	EC, β^+, β^-	666.3	0.0035
^{125}I	(59.407±0.009) d	EC	35.5	0.8011
^{127m}Te	(107±4) d	IT, β^-	88.3	0.9727
^{125m}Te	(57.4±0.2) d	IT	144.8	0.968
^{123m}Te	(119.3±0.1) d	IT	247.6	0.972
^{121m}Te	(154±7) d	IT, EC	294.0	0.842
^{121}Te	(19.16±0.05) d	EC	507.6, 573.1	0.011
^{22}Na	(2.6029±0.0008) y	EC, β^+	511	0.0050
			1274.6	0.0038

Table 1. Main cosmogenically induced isotopes identified in the data of ANAIS-25 modules. Half-lives and decay mechanisms are indicated. Fourth column shows the energy of main gamma emissions or, in the case of the metastable states, the energy of the corresponding excited level. Last column gives the considered product of intensity I and detection efficiency ϵ for the analyzed distinctive signal of each isotope (see text). Decay information is taken from [41] for ^{125}I, ^{127m}Te, ^{123m}Te and ^{22}Na and from [42] for the other isotopes.

the daughter nucleus with a half-life $T_{1/2} = (16.1 \pm 0.7)10^6$ y [41], being hence the expected signal in large NaI(Tl) crystals a continuous beta spectrum starting in 39.6 keV. This signal is above the region of interest for dark matter searches, but it is important for background understanding [29]. The long lifetime and the difficulty to disentangle the signal from other emissions are the reasons why we cannot quantify the amount of ^{129}I in ANAIS-25 crystals. In [39] the estimated fraction of this isotope was determined to be $^{129}I/^{nat}I = (1.7 \pm 0.1)10^{-13}$; however, strong variability of this concentration is expected in different origin ores.

In the case of ^{123}Te, we expect the presence of this isotope as daughter of the metastable state ^{123m}Te, effectively identified, and probably also directly produced by cosmic rays by similar reaction mechanisms. This isotope would decay 100% following EC to the ground state of the daughter nucleus, having a half-life larger than 10^{13} y [42]. The signature in ANAIS-25 detectors would be a peak corresponding to the full absorption of the binding energy of L-shells of Sb. For the moment, this signal cannot be resolved from other contributions from Te/I isotopes still present, having L-shell EC in higher or lower extent, and then quantification is not possible in ANAIS-25 data.

3 Data analysis and estimate of production rates at sea level

We analyze in the following the distinctive signatures considered for the identification of each cosmogenically induced isotope listed in table 1, as well as the estimate of the corresponding detection efficiency ϵ in ANAIS-25 set-up. When required, the efficiencies have been obtained by Geant4 simulation (version 9.4.p01) considering the complete geometry of the ANAIS-25 set-up and isotopes homogeneously distributed in the crystals; this kind of Monte Carlo simulations was validated with a similar set-up, but slightly different detector geometry, in [29] by reproducing measurements with calibration sources, finding an accuracy at the level of 10%, although a Compton/peak suppression is systematically observed in the simulations. For the metastable isotopes of Te, full energy depositions corresponding to the excited level energy have been considered. Activation has been assessed independently for each crystal, and whenever possible, results have been properly combined.

- For ^{125}I, the peak at 67.3 keV has been considered. Since this isotope decays with 100% probability by electron capture to an excited state of the Te daughter nucleus, this peak is produced by the sum of the energy of the excited level (35.5 keV) and the binding energy of the K shell of Te (31.8 keV). Efficiency for the detection of the energy deposition is expected to be ∼100%, hence the product $I\epsilon$ is taken to be equal to the K-shell EC probability, $I\epsilon$ =0.8011 [41].

- For ^{127m}Te, the peak at 88.3 keV, corresponding to the energy of the metastable state, has been analyzed. The branching ratio of the internal transition is I =97.27% [41] and 100% detection efficiency has been assumed. Signal from D1 detector could not be evaluated along data set II since a worse resolution hindered good fitting and therefore in this case final results come only from D0 detector.

- For ^{125m}Te, the peak at 144.8 keV has been studied. Internal transition occurs with 100% probability and detection efficiency has been evaluated by simulation giving ϵ =0.968. In this case, it has been possible to quantify the peak from both the low and high energy spectra, although not for all data sets and detectors; therefore, final results have been obtained only from D0 in the low energy spectrum.

- For ^{123m}Te, the peak at 247.6 keV in high energy spectra has been analyzed. The branching ratio of internal transition is 100%. The loss of efficiency due to the emission with 84% probability of a 159 keV photon [41] which can escape detection has been evaluated by Geant4 simulation giving an overall detection efficiency $I\epsilon$ =0.972.

- Similarly, for ^{121m}Te, the peak at 294.0 keV in high energy spectra has been analyzed and a correction factor to the detection efficiency has been estimated by means of Geant4 simulation to account for the probability of losing the 212 keV gamma ray which is emitted in 81% of the decays [42]. The branching ratio of internal transition is here 88.6% [42] and then the final value considered for $I\epsilon$ is 0.842.

- A coincidence technique analysis has been applied to quantify ^{126}I and ^{121}Te, which decay by electron capture to excited states of the daughter nuclei. The identifying signature is the number of coincidences produced by the full absorption of high energy gamma emissions (see table 1) in one detector and that corresponding to the binding energy for K shell electrons in Te or Sb (31.8 or 30.5 keV, respectively) in the other detector. Just as an example, figure 4 shows the coincidence plot between detectors D0 and D1, considering their high and low energy spectra respectively, obtained in the beginning of data set I. By selecting a window from 15 to 45 keV in D1 data, we obtain the D0 coincident spectrum shown in figure 4: peaks from ^{121}Te and ^{126}I are clearly observed and are used to determine the number of events attributable to each isotope in a given time period. The product $I\epsilon$ for these coincidence signals has been evaluated by simulating the decays of each isotope in the crystals with Geant4, obtaining $I\epsilon$ =0.0035 for ^{126}I and $I\epsilon$ =0.011 for ^{121}Te. These two isotopes have the shortest half-lives of all the analyzed products. The coincidence signal has been properly identified only within the first 42 days of available data for ^{126}I. However, for ^{121}Te the signal has not faded out since this isotope is being produced as result of the decay of the longer lived ^{121m}Te, also cosmogenically induced; therefore, this point has been considered in the analysis of the time evolution of the coincidence signature of ^{121}Te (see section 3.1.2).

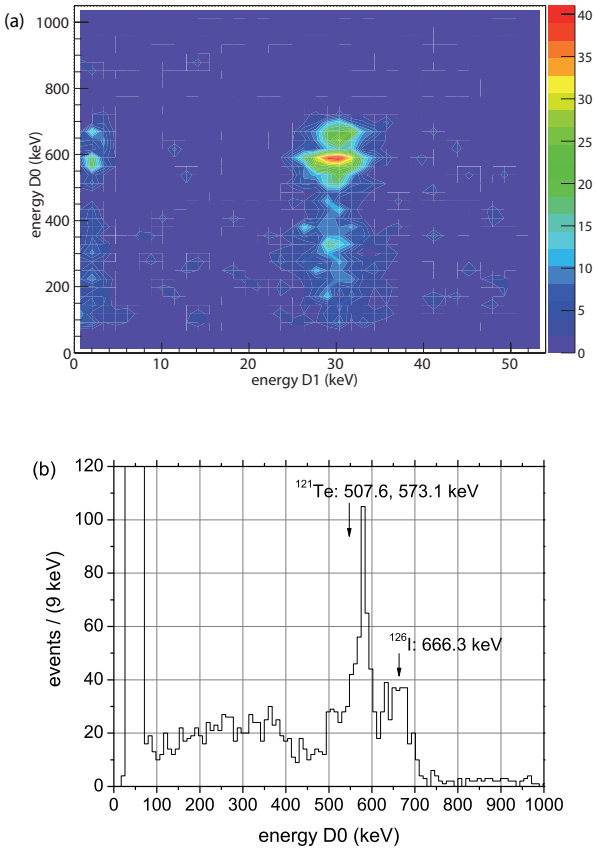


Figure 4. (a): Coincidence plot between D0 and D1 in the beginning of data set I. Coincidences due to both ^{126}I and ^{121}Te between high energy photons absorbed in D0 and the binding energies of Te or Sb registered in D1 are clearly seen, for K shell (around 31 keV) and even for L shell (around 5 keV). D0 energies below 80 keV have been cut because the high rate of coincidences there prevents from seeing ^{126}I and ^{121}Te coincidences. (b): Spectrum of the high energy D0 data in coincidence with a window in D1 data around K shell binding energies of Te and Sb; peaks at 507.6-573.1 and 666.3 keV are singled out and can be quantified.

- Presence of ^{22}Na, having a longer lifetime, is more subtle. The analyzed signal has been the integral number of events from 2300 to 2900 keV (corresponding to full absorption of its positron and gamma emissions) in the spectrum obtained summing D0 and D1 energies, for coincidence events leaving 511 (or 1275) keV at any detector. This is the best signature found for this isotope to avoid the interference of backgrounds. The product $I\epsilon$ for these signals has been evaluated by Geant4 simulation of ^{22}Na decays in the crystals, obtaining $I\epsilon$ =0.0050 for the 511 keV peak and $I\epsilon$ =0.0038 for the 1275 keV signal.

In order to quantify the cosmogenic production of every isotope identified in ANAIS-25 measurements, the cosmogenically induced activity, which is the initial activity A_0 corresponding to the moment of storing crystals deep underground at LSC, has been first deduced (section 3.1). For that, the time evolution of the identifying signature produced by each I and Te isotope has been studied considering data sets I and II; as already commented, special

analysis is required for ^{121}Te. For ^{22}Na, the integrated signal along data set III has been used. Finally, an attempt has been made to estimate production rates R_p at sea level from those A_0 activities (section 3.2), taking into account the history of crystals.

3.1 Initial activities underground

3.1.1 I and metastable Te isotopes

The evolution in time of the counting rates R for the different identifying signatures described above has been analyzed and is shown in the plots of figure 5 for I and metastable Te isotopes[3]. Single exponential decays following the radioactive decay law are clearly observed in all of them. Fits of R vs time have been carried out considering not only the sum of the signals from each detector (shown for most of the products) but also independent signals from D0 and D1, and for ^{125m}Te, even signals from the low and high energy spectra have been independently analyzed; in all cases compatible results have been obtained. From the fit parameters the half-lives $T_{1/2}$ and initial activities underground A_0 have been derived for each isotope, taking into account the described intensity I and efficiency ϵ for the considered signals, and are summarized in table 2. Error bars plotted in figure 5 represent for Y-axis the uncertainty of peak areas, which has been taken into account in the fits; for X-axis, they only indicate the time range signals have been evaluated over. As shown in table 2, the half-lives deduced from the fits agree with the known values within uncertainties, confirming the choice of signatures for each isotope.

The initial activities A_0 have been also deduced following a different approach, taking into consideration the decay of isotopes during the time intervals over which the identifying signals are integrated. For an isotope with decay time constant λ, the expected number of events C from time t_i to t_f is:

$$C = \frac{A_0 I \epsilon [\exp(-\lambda t_i) - \exp(-\lambda t_f)]}{\lambda} \tag{3.1}$$

An average of the A_0 values deduced from eq. (3.1) for each period of time has been obtained for each isotope, weighted with uncertainties coming from peak area estimates; results are shown in table 2 too. The two methods give compatible results, although slightly lower values are systematically obtained from the second one; only a larger difference is found for ^{126}I due to its shorter half-life. The advantage of deriving A_0 by fitting R vs time is that no assumption on the nature of the isotope is made, while the value from the average of the initial activities obtained from time intervals takes into account the decay of isotopes during those intervals, which is not completely negligible.

3.1.2 ^{121}Te

Figure 6 shows the evolution in time of the activity of ^{121}Te deduced from its identifying signal adding D0 and D1 data. A single exponential decay with the half-life of ^{121}Te is not observed in this case because the isotope is being produced by the decay of ^{121m}Te, also cosmogenically induced and having a longer half-life. A different fitting function is needed to derive the initial activity underground and to estimate the production rate at sea level for ^{121}Te.

[3]The origin of absolute times has been chosen at 0 h on 28^{th} November 2012, corresponding to the storage of detectors deep underground at LSC

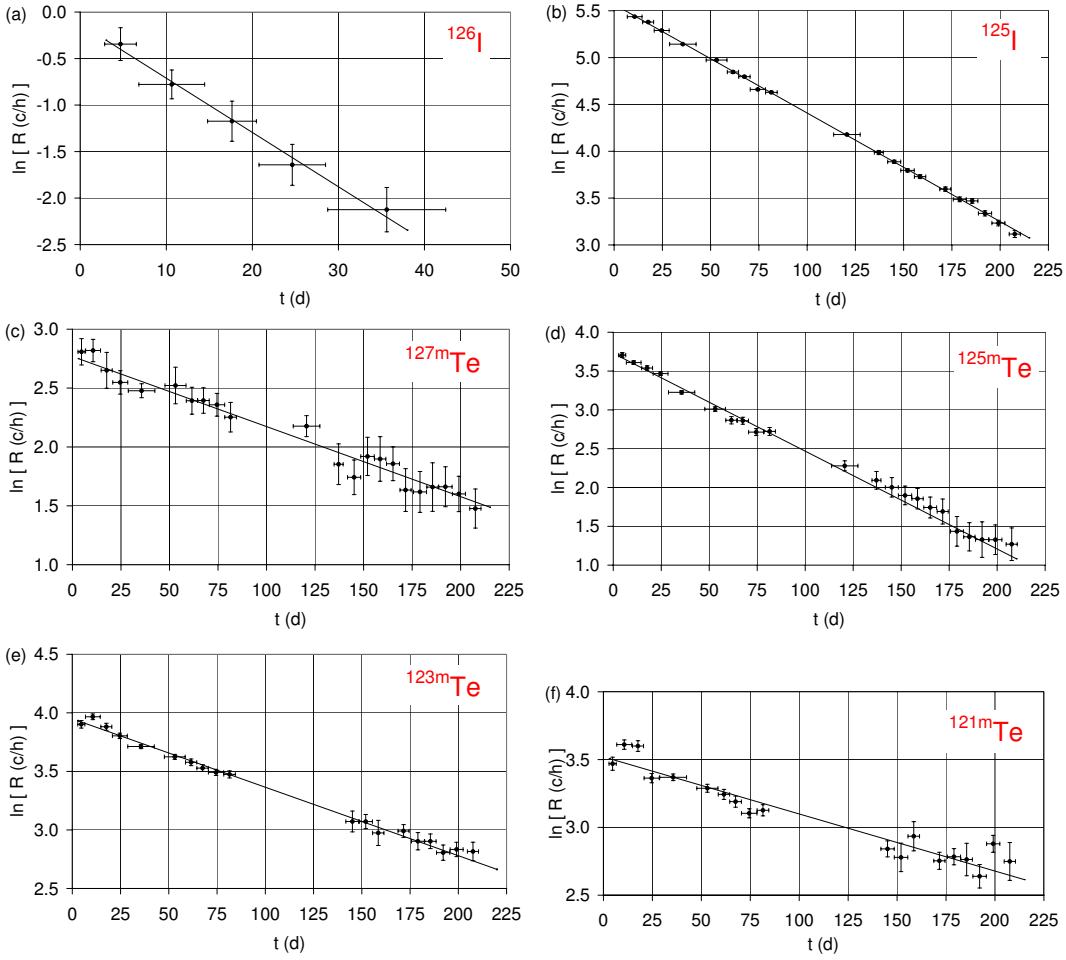


Figure 5. Evolution in time of the logarithm of the counting rate R (expressed in counts per hour) assigned to each isotope, calculated as the addition of the rates in D0 and D1 detectors. Only for ^{127m}Te (c) and ^{125m}Te (d) results correspond to rate measured with D0 detector. The corresponding fits are also shown (solid line). Error bars on X-axis only indicate the time range signals have been evaluated over.

Isotope	Known $T_{1/2}$ (days)	Detector	Data sets	Fitted $T_{1/2}$ (days)	Fitted A_0 ($kg^{-1}d^{-1}$)	Average A_0 ($kg^{-1}d^{-1}$)
^{126}I	12.93±0.05	D0+D1	I	11.9±1.7	483±77	430±37
^{125}I	59.407±0.009	D0+D1	I+II	59.80±0.26	627.6±2.4	621.8±1.6
^{127m}Te	107±4	D0	I+II	116.4±8.1	31.5±1.3	32.1±0.8
^{125m}Te	57.40±0.15	D0, LE	I+II	55.0±1.1	82.6±1.2	79.1±0.8
^{123m}Te	119.3±0.1	D0+D1	I+II	118.6±3.1	102.5±1.2	100.8±0.8
^{121m}Te	154±7	D0+D1	I+II	164.6±9.3	77.1±1.7	76.9±0.8

Table 2. Results derived for each cosmogenic product from the selected detectors and data sets: half-lives $T_{1/2}$ and initial activities underground A_0 from the fits of R vs time and average A_0 from activities obtained from time intervals considering the isotope decay (see text). The known values of the half-lives, presented in table 1, are included again for comparison.

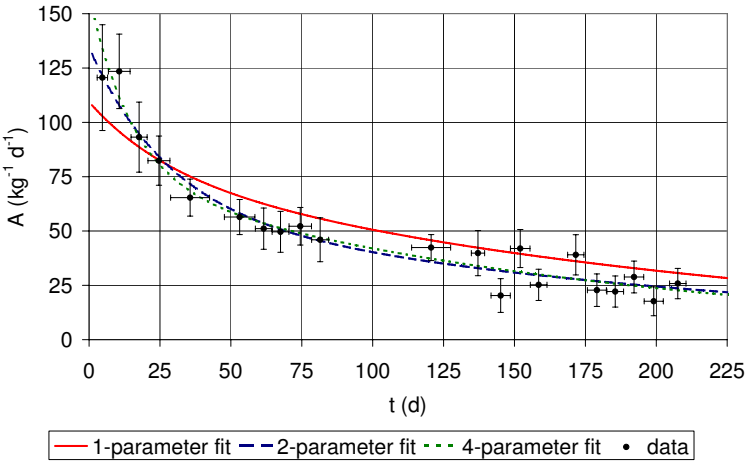


Figure 6. Evolution in time of the ^{121}Te activity deduced from the identifying signature summed from D0 and D1; the lines show the corresponding fits to eq. (3.2), considering 1 (red solid line), 2 (blue dashed line) and 4 (green dotted line) free parameters (see text).

The time dependence of the activity of ^{121}Te during the data taking in ANAIS-25 can be written as the addition of two terms, corresponding to the decay of the cosmogenically produced ^{121}Te and to the production, and subsequent decay, of ^{121}Te from ^{121m}Te:

$$A(t) = \lambda_g N_{0,g} exp(-\lambda_g t) + P_{IT} N_{0,m} \frac{\lambda_g \lambda_m}{\lambda_g - \lambda_m} [\exp(-\lambda_m t) - \exp(-\lambda_g t)] \qquad (3.2)$$

with subindex $g(m)$ referring to the ground (metastable) states of the isotope and being N_0 the initial number of nuclei (therefore those cosmogenically induced) and P_{IT} =0.886 the probability of internal transition of the metastable state. To obtain the initial number of nuclei, and then the corresponding activities, for both the ground and metastable states, several fits to the dependence given by eq. (3.2) for the signal from ^{121}Te have been tried and are also plotted in figure 6. One fit has been performed letting four parameters free: the activities $A_{0,g} = N_{0,g}\lambda_g$ and $A_{0,m} = N_{0,m}\lambda_m$ and the half-lives $T_{1/2,g}$ and $T_{1/2,m}$. Other fit has been made with two free parameters, fixing the two half-lives according to the known values reported in table 1. The last fit has been carried out with only one free parameter, fixing in addition the activity of the metastable state to the average of the two estimates given in table 2: $A_{0,m}$ =77.0 kg^{-1}d^{-1}. The product $I\epsilon$ presented in table 1 has been used. All the fit results are presented in table 3. The three estimates of the initial activity underground for ^{121}Te are reasonably compatible within uncertainties and those for ^{121m}Te are of the same order than the value deduced before (see section 3.1.1 and table 2). The half-lives deduced in the first fit reported in table 3 are in the 2σ interval of the known values. The ^{121}Te activity obtained from the 1-parameter fit (which takes into account all known information) will be used to estimate the production rate.

3.1.3 ^{22}Na

For ^{22}Na, having a much longer mean life than I and Te isotopes, the evolution in time of the identifying signal has not been studied; signal integrated along the available data in set III (88.12 days) has been considered instead.

Fit	$A_{0,m}$ ($kg^{-1}d^{-1}$)	$A_{0,g}$ ($kg^{-1}d^{-1}$)	$T_{1/2,m}$ (d)	$T_{1/2,g}$ (d)
4 parameters	76±15	159±33	122±27	10.5±5.4
2 parameters	59.3±3.9	134±13	-	-
1 parameter	-	110±12	-	-

Table 3. Initial activities underground and half-lives derived for the metastable and ground states of ^{121}Te by fitting the signal plotted in figure 6 to the dependence given by eq. (3.2) with different sets of free parameters (see text).

Signal (keV)	A ($kg^{-1}d^{-1}$) from data set III	A_0 ($kg^{-1}d^{-1}$)
511	109.0±4.3	158.2±6.3
1275	111.8±5.5	162.2±8.0
mean	110.0±3.4	159.7±4.9

Table 4. Measured activity of ^{22}Na from data set III and the deduced initial activity underground A_0, considering the identifying signal for coincident events leaving 511 or 1275 keV at one detector (see text). These activities independently estimated have been properly averaged to derive the final result.

Figure 7 (a) shows the energy spectra of D0 and D1 registered for coincidences between them for data set III. Two complementary signatures have been considered: events selected by a 511 keV (1275 keV) energy deposition in one detector (fixing a window at $\pm 1.4\sigma$) have been used to build total deposited energy spectra and then, only the region between 2300 and 2900 keV (corresponding to full absorption of its positron and gamma emissions) has been used for the rate estimate. Figure 7 (b,c) presents these total energy spectra (summing D0 and D1 energy) obtained for 511 or 1275 keV peak. The effect of coincidences not due to ^{22}Na has been taken into account subtracting their contribution in the 2300-2900 keV region, evaluated from events in a window on the left of the 511 keV peak and on the right of the 1274 keV peak. From the net number of events registered in the 2300-2900 keV region and the estimated $I\epsilon$ value reported at table 1 the activity of ^{22}Na at measuring time has been evaluated and then the initial activity underground A_0 deduced, using its half-life from table 1. Table 4 presents the results, for both 511 and 1275 keV windows; since they are compatible, they have been properly averaged. In figure 7 (b,c) the measured spectra of the summed energy of D0 and D1 are compared with the corresponding simulations normalized with the deduced ^{22}Na activity; the spectra shapes follow reasonably the expectation, somehow validating the method applied to single out ^{22}Na contribution.

3.2 Estimate of production rates at sea level

ANAIS-25 crystals were built in Alpha Spectra facilities in Grand Junction, Colorado. The history of the starting material used to produce the NaI powder from which crystals are grown is unknown; this exposure along geological time scales must be relevant only for very long-lived isotopes like ^{129}I or ^{123}Te, for those having shorter lifetimes saturation would have been probably reached independently from previous exposure history while purifying, growing the crystals and building the detectors (except maybe for ^{22}Na). Colorado is placed at a quite high altitude; consequently, a very important correction factor f to the cosmic neutron flux at New York City coordinates is reported at [43] for Colorado locations due to altitude and geomagnetic rigidity (4.11 and even 12.86 for Denver and Leadville, respectively). Afterwards,

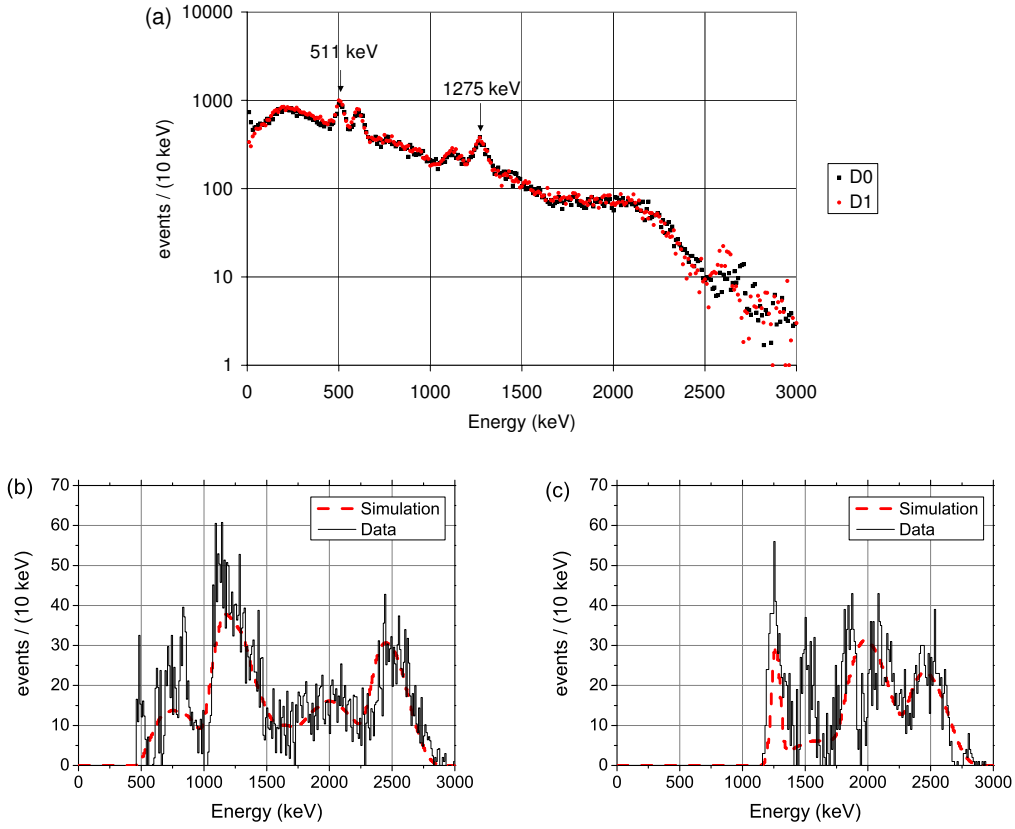


Figure 7. (a): Energy spectra of D0 (black squares) and D1 (red circles) registered for coincidences between them for data set III. (b) and (c): Spectrum of the summed energy of D0 and D1 for events in a $\pm 1.4\sigma$ window around the 511 (b) and 1275 keV (c) peaks in any of the coincidence spectra. ^{22}Na signature has been evaluated from the region between 2300 and 2900 keV (corresponding to full absorption of its positron and gamma emissions). Measured spectra are compared with simulations normalized with the deduced ^{22}Na activity.

detectors were transported to LSC by boat and by road, being the travel duration about one month, most of the time at sea level. Therefore, the initial activities underground derived in section 3.1 cannot be directly considered the saturation activities (i.e. production rates, R_p) at sea level. However, in the following a method to estimate the production rates in our crystals, based on a few reasonable assumptions, is proposed.

Considering that saturation activity is reached at a given place characterized by a correction factor f to the cosmic neutron flux at sea level, the number of nuclei cosmogenically induced for a particular isotope is $N_{sat} = fR_p/\lambda$. If the material is then exposed to cosmic rays at sea level for a time t, it is straightforward to derive the posterior evolution of the corresponding activity by solving the usual differential equation with simultaneous production and decay of a nuclear species for an initial number of nuclei N_{sat}:

$$A(t) = R_p[1 + (f - 1)\exp(-\lambda t)] \tag{3.3}$$

The production rate R_p of an isotope can be obtained from eq. (3.3) using its initial activity underground, obtained in section 3.1, and fixing the correction factor f and exposure

	Denver	Leadville
f [43]	4.11	12.86
altitude in ft (m)	5130-5690 (1564-1731)	10152 (3094)
flux ratio to Grand Junction	1.18	3.47
f at Grand Junction	3.5	3.7

Table 5. Estimate of the correction factor f for the cosmic neutron flux at Grand Junction from the factors at Denver and Leadville. The ratio between the flux at these locations and Grand Junction due to different altitude has been derived following [43]; the altitude of Grand Junction is 4593 ft (1397 m).

Isotope	R_p ($kg^{-1}d^{-1}$)
^{126}I	283±36
^{125}I	220±10
^{127m}Te	10.2±0.4
^{125m}Te	28.2±1.3
^{123m}Te	31.6±1.1
^{121m}Te	23.5±0.8
^{121}Te	9.9±3.7
^{22}Na	45.1±1.9

Table 6. Production rates at sea level R_p deduced for all the identified cosmogenic isotopes (in $kg^{-1}d^{-1}$). Values for I and metastable Te isotopes have been obtained from eq. (3.3) using the initial activities underground A_0 presented in table 2, calculated as the average values obtained for different time intervals. Rate for ground state of ^{121}Te has been deduced from eq. (3.6) using the activity in table 3 from the 1-parameter fit. For ^{22}Na, eq. (3.3) and the mean result in table 4 have been considered.

time at seal level t. Since the geographic coordinates of Grand Junction are similar to those of Denver and Leadville, their correction factors f have been adjusted to Grand Junction altitude (4593 ft=1397 m) following the method proposed in [43] (see table 5); the average of both estimates has been taken hereafter as f value. Table 6 summarizes the production rates obtained in this way for f =3.6±0.1, t =30±5 days, λ from $T_{1/2}$ values in table 1 and the A_0 values presented in tables 2 (considering the isotope decay along the data taking) and 4. Reported uncertainties include contributions from those derived for A_0 and also from λ, f and t. The relative uncertainty quantified in the production rate is $\leq$5% (except for ^{126}I); assuming much larger uncertainties in f and t, as for instance f =3.6±0.5 and t =30±10 days, increases the relative uncertainties in the production rates to $\sim$15%. Contribution from uncertainty in half-lives is negligible.

For ^{121}Te, assuming an exposure to cosmic rays in Colorado until reaching saturation followed by a short exposure at sea level (as made for the other cosmogenic products), the estimate of the production rate from the measured initial activity underground is not so easy due to the combination of direct production and production through the metastable state. In the following, $R_{p,g}$ and $R_{p,m}$ correspond to the production rates at sea level of the ground and metastable states of ^{121}Te.

At an altitude with a correction factor f for the cosmic neutron flux, the number of

nuclei N of each species is given by the system of coupled equations:

$$\begin{aligned} dN_m &= fR_{p,m}dt - \lambda_m N_m dt \\ dN_g &= fR_{p,g}dt - \lambda_g N_g dt + P_{IT}\lambda_m N_m dt \end{aligned} \tag{3.4}$$

The system in eq. (3.4) can be solved assuming that initially $N_g = N_m = 0$. Then, saturation values (for $t \to \infty$) are:

$$\begin{aligned} N_{m,sat} &= \frac{fR_{p,m}}{\lambda_m} \\ N_{g,sat} &= \frac{f(R_{p,g}+P_{IT}R_{p,m})}{\lambda_g} \end{aligned} \tag{3.5}$$

At sea level, the system of coupled equations giving the number of nuclei of ground and metastable isotopes is like that in eq. (3.4) with f =1 and can be solved assuming initially the saturation values from eq. (3.5). Then, the activity for the metastable state is given by eq. (3.3), whereas activity for the ground state is obtained as:

$$A_g(t) = (R_{p,g}+R_{p,m}P_{IT})[1+(f-1)\exp(-\lambda_g t)]+R_{p,m}P_{IT}(f-1)[\exp(-\lambda_m t)-\exp(-\lambda_g t)]\frac{\lambda_g}{\lambda_g-\lambda_m} \tag{3.6}$$

Table 6 presents the production rate at sea level $R_{p,g}$, derived from eq. (3.6), using the corresponding initial activity underground deduced in table 3 from the 1-parameter fit, the values of λ_m, λ_g and P_{IT} and the values of f and t already assumed for the other cosmogenic products. Uncertainty in the activity give the main contribution to the uncertainty in the production rate.

4 Calculation of production rates at sea level

As pointed out in section 1, cosmogenic activation of materials is an hazard for experiments looking for rare events and therefore it must be properly assessed in the background models of this type of experiments. Production rates are the main input to compute the induced activities of the relevant isotopes. Since direct estimates of the production rates, as those presented here for NaI, are not available for all materials and products, in many cases production rates must be evaluated using eq. (4.1) from the cosmic ray flux ϕ and the production cross sections σ, both dependent on the energy E of cosmic particles:

$$R_p \propto \int \sigma(E)\phi(E)dE \tag{4.1}$$

This calculation method is strongly dependent on the excitation functions and assumed cosmic ray spectrum. In order to validate different approaches to such a calculation, production rates at sea level for all the cosmogenic products identified and quantified in ANAIS-25 crystals will be evaluated and then compared with the values obtained from the measurements presented in section 3. Although not observed in ANAIS-25 data mainly due to its short half-life ($T_{1/2}$ =4.1760±0.0003 days), ^{124}I has been considered in this study too. Production rate of ^{123}Te, having low energy emissions dangerous for dark matter searches, has been also evaluated. As proposed in [5], first, all the available information on the relevant production cross sections by neutrons and protons from both measurements and calculations will be presented; then, the best description of the excitation functions of products over the whole energy range will be chosen (section 4.1). Finally, production rates considering a particular cosmic ray spectrum (section 4.2) and the selected excitation functions will be calculated and compared with the experimental values (section 4.3).

4.1 Excitation functions

The excitation function for the production of a certain isotope by nucleons in a target over a wide range of energies (from some MeV up to several GeV) can be hardly obtained only from experimental data, since the measurements of production cross-sections with beams are demanding. The use of computational codes is therefore mandatory, although experimental data are essential to check the reliability of calculations. The difficulties for properly describing excitation functions are discussed for instance at [44].

Most of the considered cosmogenic isotopes are induced by interaction on ^{127}I; only ^{22}Na is produced on ^{23}Na. Both ^{127}I and ^{23}Na have a 100% isotopic abundance in natural iodine and sodium respectively. Figures 11-18 in the appendix show the information compiled for the excitation functions of the cosmogenic products induced on ^{127}I or ^{23}Na, taken from different sources:

- The EXFOR database (CSISRS in US) [45] provided most of the experimental data. Other ones have been obtained from [46], [47] and [48].

- Libraries MENDL-2 and MENDL-2P (Medium Energy Nuclear Data Library) [49] gave results obtained by Monte Carlo simulation of the hadronic interaction between nucleons and nuclei using codes of the ALICE family, for neutrons up to 100 MeV and protons up to 200 MeV.

- At library TENDL-2013 (TALYS-based Evaluated Nuclear Data Library) [50], cross sections obtained with the TALYS nuclear model code system were found for neutrons and protons up to 200 MeV. An outstanding feature of this library is that production of metastable and ground states is evaluated separately.

- The YIELDX routine was used to compute production cross section at the whole energy range. This routine implements the most updated version of the popular Silberberg & Tsao semiempirical formulae [51]-[53] giving nucleon-nucleus cross sections for different reactions. They can be used for a wide range of targets and products at energies above 100 MeV; since they are based only on proton-induced reactions, cross section must be assumed to be the same for neutrons and protons.

- Library HEAD-2009 (High Energy Activation Data) [54] merges data for neutrons and protons up to 1 GeV. Here, data from HEPAD-2008 (High-Energy Proton Activation Data) sub-library have been considered, obtained using a selection of models and codes (CEM03.01, CASCADE/INPE, MCNPX 2.6.0,...) dictated by an extensive comparison with EXFOR data.

At low energies (LE, below 200 MeV) excitation functions for protons and neutrons are clearly different, from both MENDL and TENDL-2013 data; therefore, it is very important to quantify cosmogenic yields considering cross sections specifically evaluated for neutrons. For I isotopes, experimental data on cross sections are abundant and are in general in reasonable agreement with the excitation functions provided by MENDL, TENDL-2013, YIELDX and HEAD-2009. However, for Te isotopes, experimental information is scarce. It is worth noting that some measurements distinguish production cross sections for ground (G) or metastable (M) states of Te isotopes, but this is not the case for the considered calculations except for TENDL-2013.

Isotope	HEAD-2009		YIELDX		MENDL-2		TENDL-2013(n)	
	F	N	F	N	F	N	F	N
^{126}I	1.3	18	1.2	25	1.4	37	1.4	38
^{125}I	1.3	8	2.1	12	1.7	1	1.1	1
^{124}I	1.4	12	1.5	19	2.9	6	3.9	6
^{127m}Te	11.5	2			1.9	3	1.5	3
^{125m}Te							5.6	1
^{123m}Te	1.2	4	2.4	6				
^{121m}Te	1.1	4	1.8	6				
^{121}Te	1.7	4	1.4	6				
^{22}Na			1.2	19			1.8	107
all	1.4*	50	1.5	93	1.6	47	1.8	160

(*)Excluding the large deviation factor obtained for ^{127m}Te.

Table 7. Deviation factors F calculated following eq. (4.2) between measured production cross-sections and results from HEAD-2009 (150-1000 MeV), YIELDX (>100 MeV), MENDL-2 (<100 MeV) and TENDL-2013 for neutrons (<200 MeV). The number N of pairs used in the comparison is indicated for each case. Overall values of F have been obtained considering data for all the isotopes.

To quantify the agreement between the available experimental data and the different calculations helps to choose the best description of the excitation functions. For that, deviation factors F have been evaluated following a definition typically used in the literature:

$$F = 10^{\sqrt{d}}, \qquad d = \frac{1}{N}\sum_i (\log \sigma_{exp,i} - \log \sigma_{cal,i})^2 \tag{4.2}$$

being N the number of pairs of experimental and calculated cross sections $\sigma_{exp,i}$ and $\sigma_{cal,i}$ at the same energies. Parameter d is the mean square logarithmic deviation. Table 7 presents the obtained values for each isotope and considering all of them altogether; only proton data can be considered for HEAD-2009 and YIELDX while data for neutrons are used for MENDL-2 and TENDL-2013 calculations. Only an abnormally large deviation factor above 10 has been found for ^{127m}Te and HEAD-2009 calculation, predicting very low production cross sections well below available measurements for both metastable and ground states. Calculations at high energy show slightly better deviation factors than at low enegies; in the overall results not very significant differences are found between HEAD-2009 and YIELDX nor between MENLD-2 and TENDL-2013.

Different descriptions of the excitation functions have been analyzed for the calculation of production rates, based on the available data and calculations at the low and high energy ranges:

- For iodine isotopes, thanks to the large amount of experimental data available, the description could be fixed for each isotope following the lowest deviation factors at low and high energies according to table 7.
- For tellurium isotopes, TENDL-2013 data for neutrons were always considered below 200 MeV, since they have been calculated separately for metastable states; HEAD-2009 data, having better deviation factors than YIELDX, were used above that energy for most of the isotopes. For ^{127m}Te, it was preferred to extrapolate the TENDL-2013 value at 200 MeV to higher energies. The branching ratios for the production at

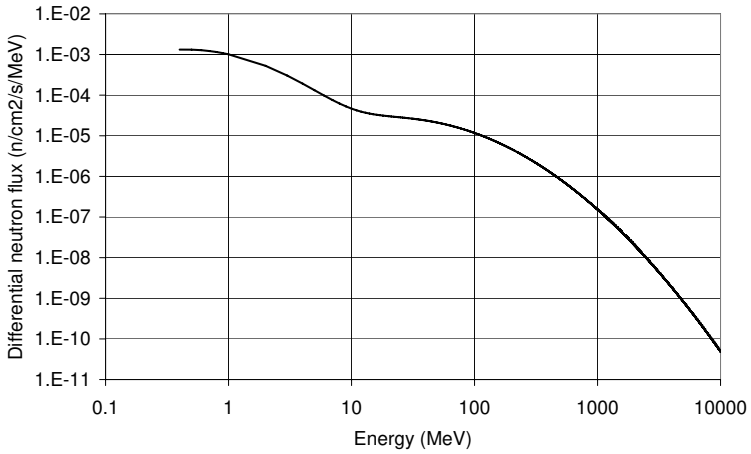


Figure 8. Energy spectrum of cosmic neutrons following the analytic expression in [56] (for conditions of New York City at sea level) which has been considered in this work to calculate production rates of cosmogenic isotopes.

ground or metastable state given by TENDL-2013 data at 200 MeV (∼0.7 for metastable production for all the considered isotopes) have been applied to data at higher energies, which do not distinguish between ground or metastable final states.

- Regarding ^{22}Na, the only description possible was using TENDL-2013 at low energies and YIELDX results at high energies.

4.2 Cosmic rays spectrum

Following eq. (4.1), the other ingredient required to evaluate production rates, together with the excitation function, is the cosmic ray spectrum. Different forms of the neutron spectrum at sea level have been used in cosmogenic activation studies, like the historical Hess spectrum [55], that proposed by Lal & Peters [1] or the parametrization based on a compilation of measurements presented by Ziegler [43]. In [56], a set of measurements of cosmic neutrons on the ground across the US was accomplished using Bonner sphere spectrometers; an analytic expression fitting data for energies above 0.4 MeV was proposed and has been considered in this work. Figure 8 shows the energy spectrum given by this description of cosmic neutrons; applied to conditions of New York City at sea level, the integral flux from 10 MeV to 10 GeV is 3.6×10^{-3}cm^{-2}s^{-1}.

4.3 Production rates

Table 8 presents the obtained production rates for the analyzed cosmogenic isotopes considering the selected excitation functions. Results are given per day and per kg of NaI. Contributions from the LE and HE descriptions of the cross sections are shown together with the total rate. For most of the isotopes, the dominant contribution comes from the low energy region; for instance, for iodine isotopes it accounts for ∼90% of the rate.

Table 8 shows also the production rates deduced experimentally in section 3.2 for comparison. Ratios between the calculated and experimental rates are given too. Most of the calculated production rates are larger than the experimental ones. Good agreement has been found for I isotopes, having cross sections well validated not only at high energy with protons

Isotope	Excitation function LE+HE	Calculated rate LE+HE	total	Experimental rate	Cal/Exp
^{126}I	MENDL-2+YIELDX	250.0+47.0	297.0	283±36	1.1
^{125}I	TENDL-2013+HEAD-2009	230.2+12.1	242.3	220±10	1.1
^{124}I	MENDL-2+HEAD-2009	113.6+22.3	135.9		
^{127m}Te	TENDL-2013+extrapolation	6.9+0.2	7.1	10.2±0.4	0.7
^{125m}Te	TENDL-2013+HEAD-2009	38.4+3.5	41.9	28.2±1.3	1.5
^{123m}Te	TENDL-2013+HEAD-2009	29.5+3.7	33.2	31.6±1.1	1.1
^{123}Te	TENDL-2013+HEAD-2009	8.8+1.4	10.2		
^{121m}Te	TENDL-2013+HEAD-2009	19.1+4.7	23.8	23.5±0.8	1.0
^{121}Te	TENDL-2013+YIELDX	5.8+2.6	8.4	9.9±3.7	0.8
^{22}Na	TENDL-2013+YIELDX	43.2+10.4	53.6	45.1±1.9	1.2

Table 8. Production rates (in kg^{-1}d^{-1}) calculated from eq. (4.1) using different selections of the excitation function (indicated in the second column) showing the contributions from LE and HE ranges and the total rate. Production rates obtained experimentally in table 6 are shown for comparison. Last column presents the ratio between the calculated and the experimental rates.

but also at low energies with neutrons. The largest deviation is obtained for ^{125m}Te; the lack of experimental data in the whole energy range (see Fig. 15) makes difficult try to improve the selection of the excitation function. For ^{22}Na, there is an important step in the description of the excitation curve at LE and HE regions (see Fig. 18) and then contribution from HE could be overestimated and/or that from LE undervalued, justifying the difference between the calculated and experimental rates; in any case, they are compatible with the calculated maximum rate of $\simeq$ 100 kg^{-1}d^{-1} at sea level quoted in [39]. The fact of observing a rate below the calculation could indicate that saturation was indeed not reached for this isotope. There is a similar mismatch in the description of the excitation function at LE and HE regions for ^{121}Te (see Fig. 17); but in this case re-scaling the curves would give production rates still compatible with the observed value.

Given the discrepancies found between calculated and experimental production rates, it can be concluded that calculations of activation yields in sodium iodide for ultra-low background experiments are precise enough, provided the used cross sections are well validated along all the relevant energy range.

5 Contribution to detector background levels

The impact of the cosmogenic isotopes produced in NaI(Tl) crystals on the background levels at the energy regions relevant for rare event searches, mainly the direct detection of WIMPs, has been assessed by means of Monte Carlo simulation. The same Geant4 application developed for the ANAIS-25 set-up and used to determine detection efficiencies (see section 3) has been used. The Radioactive Decay Model in Geant4 has been considered to reproduce the radioactive decays of the products.

Figure 9 presents the simulated spectra for each identified nuclide considering the measured initial activities underground A_0 from tables 2, 3 and 4; three different energy ranges are shown, including the very low energy region where dark matter signals are expected to appear. The total contribution from these cosmogenic isotopes has been evaluated and it is depicted in figure 10. A detailed background model of ANAIS-25 is underway (very first

results can be found in [38]); the inclusion of the contribution of cosmogenically produced isotopes is essential to properly reproduce the data taken in the first months, especially at medium and low energy [38]. As it can be observed in Figures 9 and 10, background rates at the level of several counts/keV/kg/day are coming from the identified isotopes.

In figure 10 the total contribution to the background is also compared with the one obtained considering one and five years of cooling underground. It can be concluded that although initially the contribution to the detector background level is very important, after five years the effect of cosmogenic products is completely negligible except for ^{22}Na. This isotope contributes to the whole energy region up to almost 3 MeV and gives, following the electron capture decay, a peak at 0.87 keV (the binding energy of K-shell in neon). Below 10 keV, the estimated contribution of ^{22}Na from the simulation is 5.6 kg^{-1}d^{-1} considering the initial activity A_0; after one (five) years, this rate is reduced to 4.3 (1.5) kg^{-1}d^{-1}. It must be noted that a further reduction in these values of a factor 2.5 is foreseen by anticoincidence event selection, according to simulation of a set-up with 20 detectors like those of ANAIS-25. As a reference, contribution from the measured level of ^{40}K in ANAIS-25 crystals is 5.0 kg^{-1}d^{-1} peaked at 3.2 keV.

In this study, decay of ^{123}Te has not been taken into account since the upper limit set to its half-life is very large. Nevertheless, since it could affect the very low energy region, it has been checked that considering the production rates deduced in table 8 for both metastable and ground states, for an exposure lower than 10^{10} y, present activity should be lower than 0.03 kg^{-1}d^{-1}.

6 Conclusions

Cosmogenic activation in NaI(Tl) crystals has been evaluated from the measurements taken at LSC using two 12.5 kg NaI(Tl) detectors produced by Alpha Spectra, in Colorado (US), and then shipped to Spain. The prompt data taking starting, the low radioactive background conditions and the very good energy resolution of the detectors made possible a reliable quantification of production of isotopes with half-lives larger than ten days.

Signatures from ^{125}I, ^{127m}Te, ^{125m}Te, ^{123m}Te and ^{121m}Te were directly identified in the energy spectra registered by the detectors while production of ^{126}I, ^{121}Te and ^{22}Na was revealed by analyzing coincidences between both detectors. The evolution of the identifying signature of all these isotopes, except ^{22}Na, for a period of 210 days, following the expected exponential decay, allowed to confirm the hypothesized origin of the cosmogenic signals and to evaluate the activities at the start of the underground storage. Signal from ^{22}Na was obtained from spectra taken after fifteen months. Independent analysis performed for each detector or different data sets and following different methodology gave compatible results within uncertainties. Tables 2-4 summarize the measured initial activity underground for all the observed cosmogenic products. Production rates at sea level were estimated from these activities considering that saturation was reached during detector production in Colorado (assuming a cosmic neutron flux 3.6 times higher than at sea level) and that detectors were further exposed for 30 days during the trip by boat from US to Spain. The hypothesis of saturation is reasonable for the short-lived isotopes analyzed. Results are presented in table 6. The analysis of the evolution in time of ^{121}Te signal was not so easy because direct production and production from the metastable state, also cosmogenically induced with a longer life time, were combined. Values for the metastable isotope deduced in this analysis were compatible with those obtained directly from the ^{121m}Te signature.

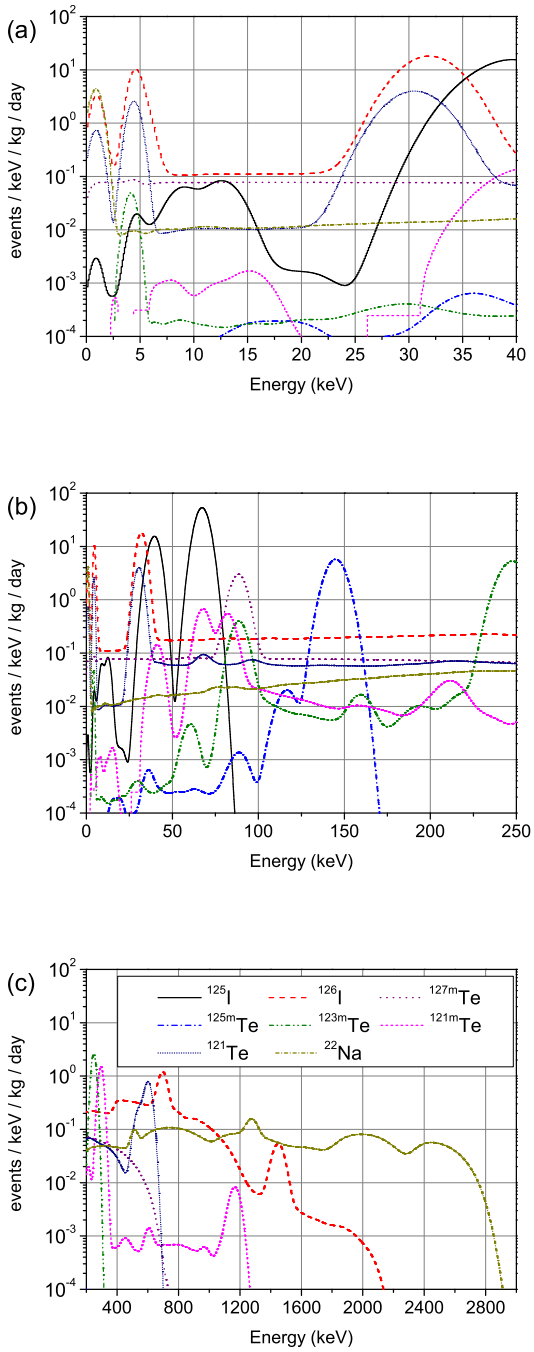


Figure 9. Background contribution from each identified cosmogenic isotope obtained by Geant4 simulation of ANAIS-25 set-up assuming the measured initial activities A_0 in three different energy ranges: (a) very low energy (below 40 keV), (b) medium energy (below 250 keV) and (c) high energy (from 200 to 3000 keV). The same legend applies to the three plots.

Calculations of production rates for all the cosmogenic isotopes observed were carried out considering the cosmic neutron spectrum given in [56] and selecting carefully the excita-

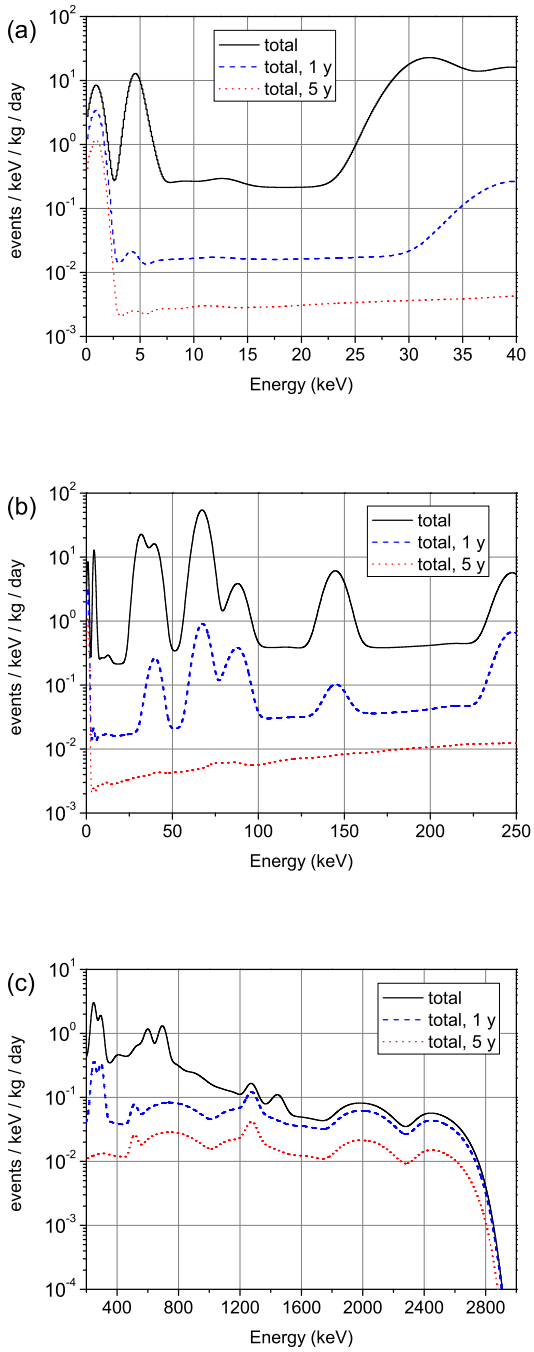


Figure 10. Sum of the background contributions depicted in Figure 9 (black). The evolution of this cosmogenic background is shown after one year (blue) and five years (red). ^{22}Na contribution is dominating the latter.

tion functions. For each product, the available information on production cross sections by neutrons and protons was collected, considering measurements, results compiled in different

libraries and calculations from semiempirical formulae made on purpose. Data from MENDL-2 or TENDL-2013 for neutrons were considered below 100 or 200 MeV while at higher energies YIELDX calculations or results from the HEAD-2009 library were used. For the analyzed isotopes, the overall deviation factors range from 1.4 to 1.8, being slightly better at high energies. Calculated production rates are summarized in table 8; agreement with the rates experimentally deduced is very good for some of the products, having excitation functions well validated against measurements. This comparison allows to quantify the systematic uncertainty when applying the followed methodology to the study of other cosmogenic products. Uncertainties in this kind of calculations come mainly from the difficulties encountered on the accurate description of cosmic ray spectra, on the precise evaluation of inclusive production cross-sections in all the relevant energy range and on the good knowledge of the material history; the low and medium energy regions below a few hundreds of MeV are the most problematic ones since neutron data are scarce and differences between neutron and proton cross sections may be important.

Some of the cosmogenic isotopes observed in this study generate emissions which could affect the very low energy region where dark matter signal is expected to appear in NaI(Tl) detectors. The contribution of all the identified products on the background level of ANAIS-25 has been evaluated by Geant4 simulation, considering the measured initial activities and those after one or five years (see figures 9 and 10). Only ^{22}Na is relevant in the long term, affecting the whole energy range and producing a peak around 0.9 keV. The other products have mean lives low enough to decay in reasonable times and they will not be a problem for dark matter detection provided crystals are left to cool underground before starting data taking.

Acknowledgments

We deeply acknowledge C. H. Tsao for providing the YIELDX routine and Yu. A. Korovin for sharing the HEAD-2009 library. This work has been supported by the Spanish Ministerio de Economía y Competitividad and the European Regional Development Fund (MINECO-FEDER) (FPA2011-23749), the Consolider-Ingenio 2010 Programme under grants MULTI-DARK CSD2009-00064 and CPAN CSD2007-00042, and the Gobierno de Aragón (Group in Nuclear and Astroparticle Physics, ARAID Foundation and C. Cuesta predoctoral grant). C. Ginestra and P. Villar are supported by the MINECO Subprograma de Formación de Personal Investigador. We also acknowledge LSC and GIFNA staff for their support.

References

[1] D. Lal and B. Peters, *Cosmic ray produced radioactivity on the Earth*, Springer, Berlin-Heidelberg (1967).

[2] G. Heusser, *Low-radioactivity background techniques*, *Annu. Rev. Nucl. Part. Sci.* **45** (1995) 543.

[3] J. A. Formaggio and C. J. Martoff, *Backgrounds to sensitive experiments underground*, *Annu. Rev. Nucl. Part. Sci.* **54** (2004) 361.

[4] P. Gondolo, *Wanted! Nuclear Data for Dark Matter Astrophysics*, to appear in Nuclear Data Sheets, arXiv:1311.6038[nucl-ex].

[5] S. Cebrián, *Cosmogenic activation of materials*, *AIP Conf. Proc.* **1549** (2013) 136-141.

[6] F. T. Avignone et al., *Theoretical and experimental investigation of cosmogenic radioisotope production in germanium*, *Nucl. Phys. B (Proc. Suppl.)* **28A** (1992) 280.

[7] H. Miley et al., *New techniques and results in ^{76}Ge double-beta decay*, *Nucl. Phys. B (Proc. Suppl.)* **28A** (1992) 212.

[8] E. B. Norman et al., *Cosmic-Ray Production of Co-60 in Double Beta-Decay Source Materials*, *Nucl. Phys. B (Proc. Suppl.)* **143** (2005) 508.

[9] I. Barabanov et al., *Cosmogenic activation of germanium and its reduction for low background experiments*, *Nucl. Instrum. Meth. B* **251** (2006) 115–120.

[10] D. M. Mei et al., *Cosmogenic production as a background in searching for Rare Physics processes*, *Astropart. Phys.* **31** (2009) 417–420.

[11] S. R. Elliott et al., *Fast-neutron activation of long-lived isotopes in enriched Ge*, *Phys. Rev. C* **82** (2010) 054610.

[12] S. Cebrián et al., *Cosmogenic activation in germanium and copper for rare event searches*, *Astropart. Phys.* **33** (2010) 316–329.

[13] M. Laubenstein, G. Heusser, *Cosmogenic radionuclides in metals as indicator for sea level exposure history*, *App. Rad. Isot.* **67** (2009) 750–754.

[14] W. Maneschg et al., *Measurements of extremely low radioactivity levels in stainless steel for GERDA*, *Nucl. Instrum. Meth. A* **593** (2008) 448–453.

[15] A. F. Barghouty et al., *Measurements of p-induced radionuclide production cross sections to evaluate cosmic-ray activation of Te*, *Nucl. Instrum. Meth. B* **295** (2013) 16–21.

[16] V. Lozza and J. Petzoldt, *Cosmogenic activation of a natural tellurium target*, *Astropart. Phys.* **61** (2015) 62–71.

[17] O. Lebeda et al., *Excitation functions of proton-induced reactions on natural Nd in the 10-30 MeV energy range, and production of radionuclides relevant for double-beta decay*, *Phys. Rev. C* **85** (2012) 014602 .

[18] O. Lebeda et al., *Excitation functions of proton-induced reactions on natural Nd and production of radionuclides relevant for double beta decay: Completing measurement in 5-35 MeV energy range*, *Nucl. Phys. A* **929** (2014) 129–142.

[19] J.B. Birks, *The Theory and Practice of Scintillation Counting*, Pergamon Press Ltd. (1964).

[20] P. Lecoq, A. Annenkov, A. Gektin, M. Korzhik, C. Pedrini, *Inorganic Scintillators for Detector Systems*, Springer-Verlag, Berlin-Heidelberg (2006).

[21] K. Fushimi et al., *Application of a large volume NaI scintillator to search for dark matter*, *Phys. Rev. C* **47** (1993) 425;
K. Fushimi et al., *Limits on the annual modulation of WIMPs-nucleus scattering with large volume NaI(Tl) scintillators*, *Astropart. Phys.* **12** (1999) 185.

[22] M.L. Sarsa et al., *Searching for annual modulations of WIMPs with NaI scintillators*, *Phys. Lett. B* **386** (1996) 458;
M.L.Sarsa et al., *Results of a search for annual modulation of WIMP signals*, *Phys. Rev. D* **56** (1997) 1856.

[23] R. Bernabei et al., *On a further search for a yearly modulation of the rate in particle dark matter direct search*, *Phys. Lett. B* **450** (1999) 448;
R. Bernabei et al., *Performances of the 100 kg NaI (Tl) set-up of the DAMA experiment at Gran Sasso*, *Riv. Nuovo Cim. A* **112** (1999) 545.

[24] G. Gerbier et al., *Pulse shape discrimination and dark matter search with NaI (Tl) scintillator*, *Astropart. Phys.* **11** (1999) 287.

[25] G.J. Alner et al., *Limits on WIMP cross-sections from the NAIAD experiment at the Boulby Underground Laboratory*, *Phys. Lett. B* **616** (2005) 17.

[26] K. Fushimi et al., *PICO-LON Dark Matter Search*, *J. Phys.: Conf. Ser.* **469** (2013) 012011.

[27] R. Bernabei et al., *Final model independent result of DAMA/LIBRA-phase 1*, *Eur. Phys. J. C* **73** (2013) 2648.

[28] J. Amaré et al., *From ANAIS-25 towards ANAIS-250*, arXiv:1404.3564.

[29] S. Cebrián et al., *Background model for a NaI(Tl) detector devoted to dark matter searches*, *Astropart. Phys.* **37** (2012) 60.

[30] C. Cuesta et al., *Analysis of the ^{40}K contamination in NaI(Tl) crystals from different providers*, *Int. J. Mod. Phys. A* **29** (2014) 1443010.

[31] C. Cuesta et al., *Slow scintillation time constants in NaI(Tl) for different interacting particles*, *Opt. Mat.* **36** (2013) 316.

[32] C. Cuesta et al., *Bulk NaI(Tl) scintillation low energy events selection with the ANAIS-0 module*, *Eur. Phys. J. C* **74** (2014) 3150.

[33] J. Cherwinka et al., *First Data from DM-Ice17*, *Phys. Rev. D* **90** (2014) 092005.

[34] K. W. Kim et al., *Tests on NaI(Tl) crystals for WIMP search at Yangyang Underground Laboratory*, *Astropart. Phys.* **62** (2015) 249-257.

[35] E. Shields, SABRE collaboration, *SABRE: A new NaI(Tl) dark matter direct detection experiment*, contribution at TAUP2013, Asilomar, US, September 2013.

[36] V. Kudryavtsev, M. Robinson, N.J.C. Spooner, *The expected background spectrum in NaI dark matter detectors and the DAMA result*, *Astropart. Phys.* **33** (2010) 91Ũ96.

[37] R. Bernabei et al., *Technical aspects and dark matter searches*, *J. Phys. Conf. Ser.* **203** (2010) 012040.

[38] C. Cuesta et al., *Preliminary results of ANAIS-25*, *Nucl. Instrum. Meth. A* **742** (2014) 187-190.

[39] R. Bernabei et al., *The DAMA/LIBRA apparatus*, *Nucl. Instrum. Meth. A* **592** (2008) 297-315.

[40] J. Amaré et al., *ANAIS: Status and prospects*, arXiv:1410.5949.

[41] Decay Data Evaluation Projet, http://www.nucleide.org/DDEP_WG/DDEPdata.htm.

[42] WWW Table of Radioactive Isotopes, http://ie.lbl.gov/toi/.

[43] J. F. Ziegler, *Terrestrial cosmic ray intensities*, *IBM J. Res. Develop.* **42** (1998) 117.

[44] R. C. Reedy, *Cosmogenic-nuclide production rates: Reaction cross section update*, *Nucl. Instrum. Meth. B* **294** (2013) 470-474.

[45] http://www.nndc.bnl.gov/exfor/exfor.htm, http://www-nds.iaea.org/exfor/exfor.htm

[46] C. S. Dyer et al., *Calculation of radioactivity induced in gamma-ray spectrometers during spaceflight*, *Nucl. Instrum. Meth. A* **173** (1980) 585-601.

[47] V. S. Pronskikh et al., *Study of proton induced reactions in a radioactive ^{129}I target at E_p =660 MeV*, [arXiv:nucl-ex/0403056].

[48] J. Vrzalová et al., *Studies of (n,xn) cross-sections in Al, Au, Bi, Cu, Fe, I, In, Mg, Ni, Ta, Y, and Zn by the activation method*, *Nucl. Instrum. Meth. A* **726** (2013) 84-90.

[49] http://www-nds.iaea.org/publications/iaea-nds/iaea-nds-0136.htm, http://www.oecd-nea.org/tools/abstract/detail/iaea1376.

[50] http://www.talys.eu/tendl-2013.html, A.J. Koning and D. Rochman, *Modern Nuclear Data Evaluation With The TALYS Code System*, *Nuclear Data Sheets* **113** (2012) 2841-2934.

[51] R. Silberberg and C. H. Tsao, *Partial cross-sections in high-energy nuclear reactions, and astrophysical applications*, *Astrophys. J. Suppl. Ser.* **25** (1973) 315; ibid p. 335.

[52] R. Silberberg and C. H. Tsao, *Cross sections for (p,xn) reactions, and astrophysical applications*, *Astrophys. J. Suppl. Ser.* **35** (1977) 129.

[53] R. Silberberg and C. H. Tsao, *Updated partial cross sections for proton-nucleus reactions*, *Astrophys. J.* **501** (1998) 911.

[54] Yu. A. Korovin et al., *High Energy Activation Data library (HEAD-2009)*, *Nucl. Instrum. Meth. A* **624** (2010) 20-26.

[55] W. N. Hess et al., *Cosmic-ray neutron energy spectrum*, *Phys. Rev.* **116** (1959) 445.

[56] M. S. Gordon et al., *Measurement of the flux and energy spectrum of cosmic-ray induced neutrons on the ground*, *IEEE Transactions on Nuclear Science* **51** (2004) 3427.

A Excitation functions

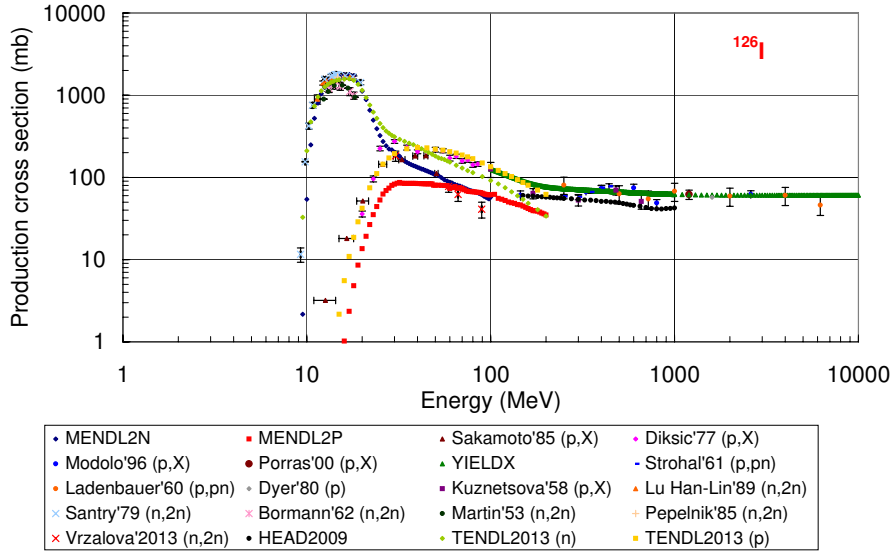


Figure 11. Comparison of excitation functions for production of ^{126}I on ^{127}I by nucleons (neutrons are indicated as n and protons as p) taken from different sources (see text).

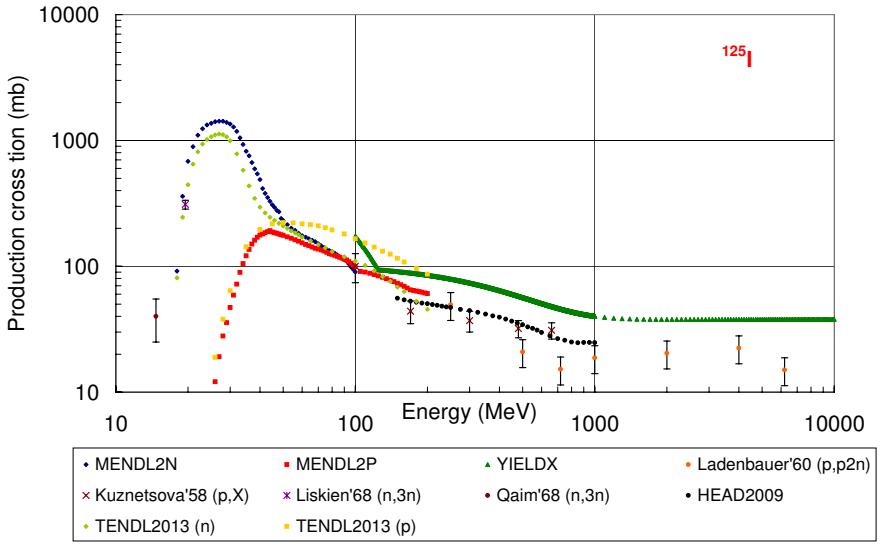


Figure 12. As figure 11, for ^{125}I.

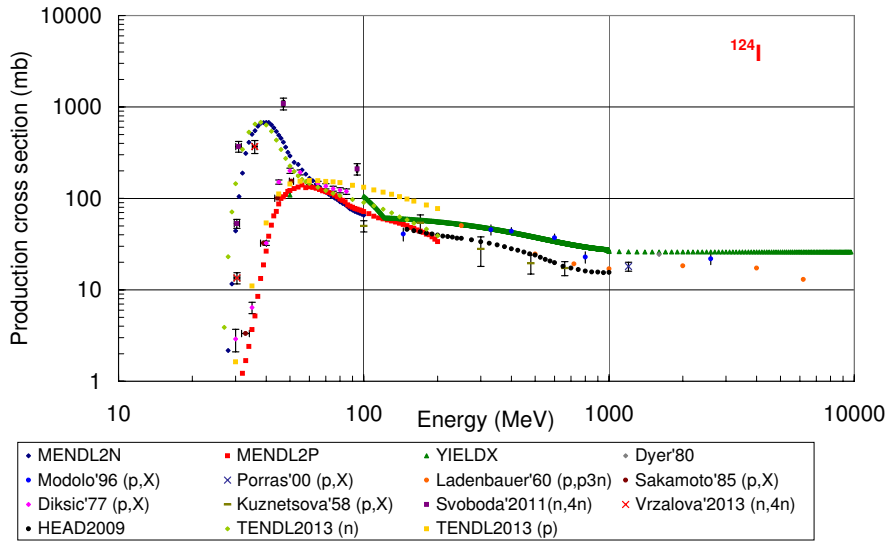


Figure 13. As figure 11, for ^{124}I.

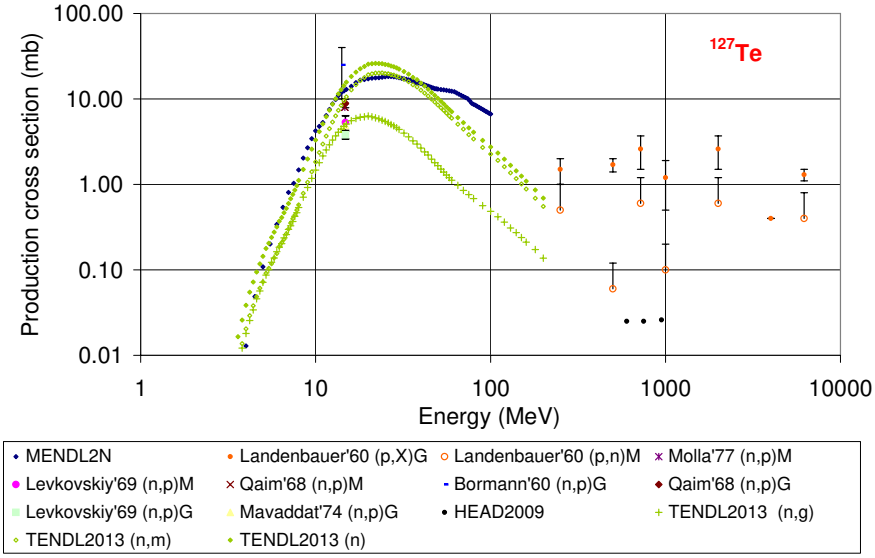


Figure 14. As figure 11, for ^{127}Te.

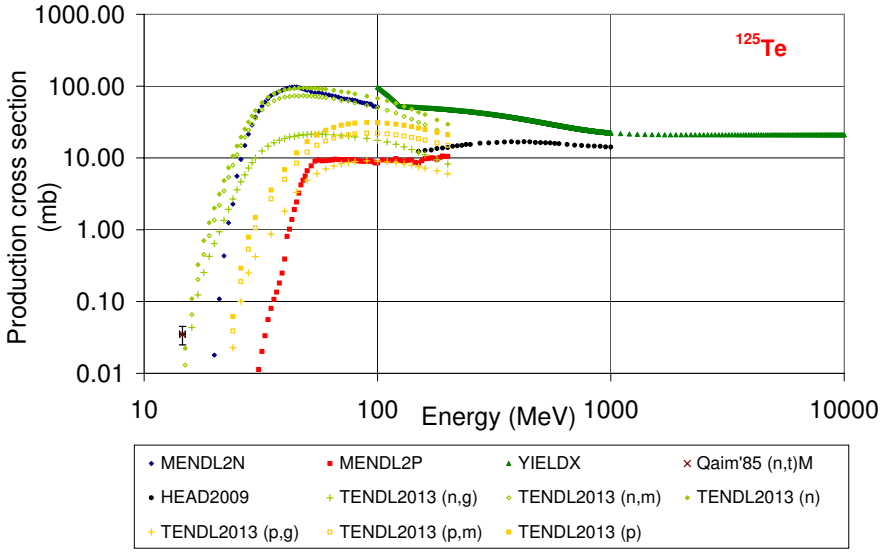


Figure 15. As figure 11, for ^{125}Te.

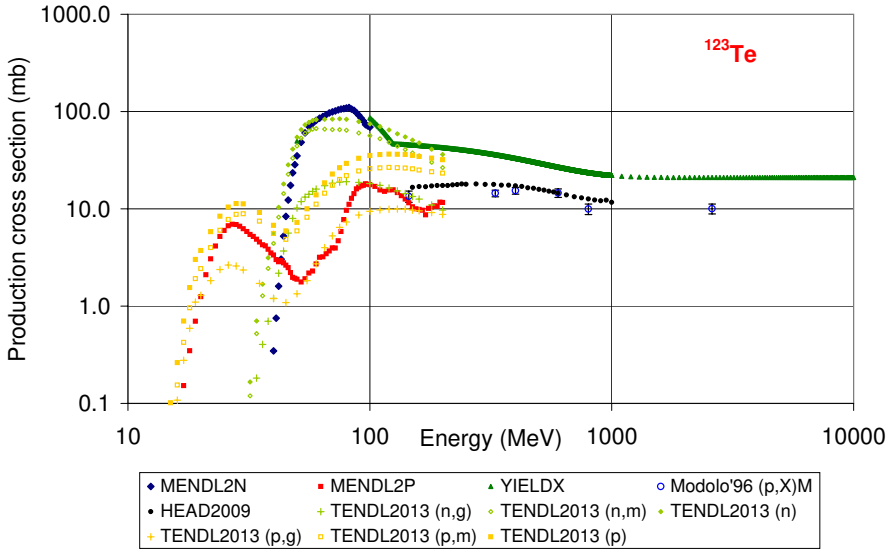


Figure 16. As figure 11, for ^{123}Te.

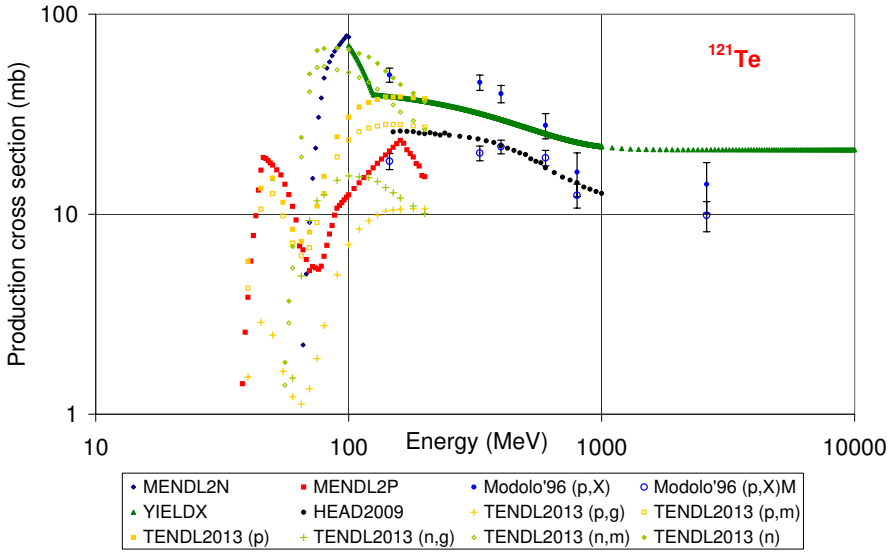


Figure 17. As figure 11, for ^{121}Te.

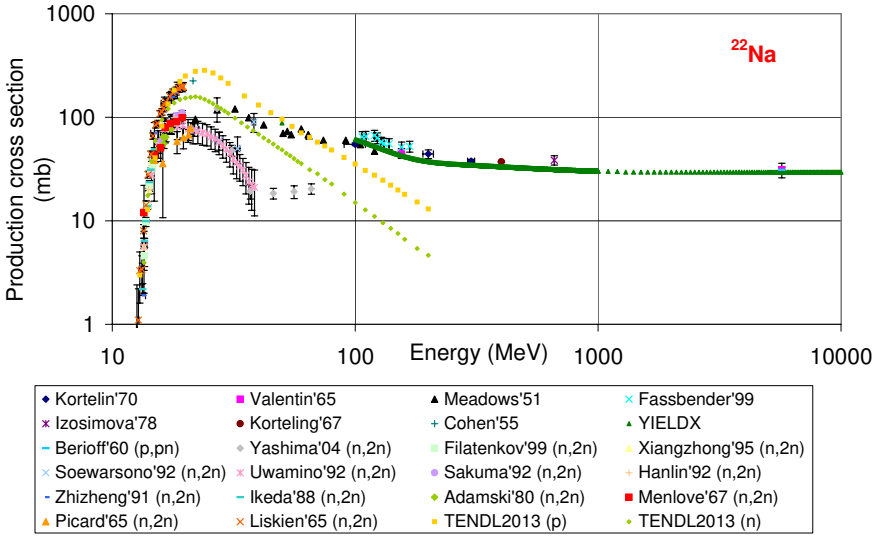


Figure 18. As figure 11, for production of ^{22}Na on ^{23}Na.